# Period-doubling and Hopf bifurcations in far-infrared driven quantum well intersubband transitions

Adriano A. Batista,[1] Bjorn Birnir,[2] P. I. Tamborenea,[3] and D. S. Citrin[1]
[1]*School of Electrical and Computer Engineering, Georgia Institute of Technology, Atlanta, Georgia 30332-0250, USA*
[2]*Mathematics Department, University of California, Santa Barbara, California 93106, USA and Science Institute, University of Iceland, 107 Reykjavik, Iceland*
[3]*Departamento de Fisica, FCEN, Universidad de Buenos Aires, (1428) Buenos Aires, Argentina*
(Received 4 February 2003; published 7 July 2003)

The behavior of $n$-$\delta$-doped wide quantum well (QW) heterostructures in the presence of intense far-infrared (FIR) radiation is studied using the semiconductor Bloch equations, in the time-dependent Hartree version and without the rotating-wave approximation. A QW is designed where one can either obtain a strong subharmonic (period doubling) or a strong incommensurate (Hopf) frequency response by varying the sheet density and field strength. These strong responses should be attainable with current technology, and the field amplitudes and frequencies of the drive are well within the range of FIR free-electron lasers.

DOI: 10.1103/PhysRevB.68.035307 PACS number(s): 78.67.De, 05.45.−a, 42.65.Sf, 73.21.Fg

The incommensurate-frequency response [due to Hopf bifurcations (HB's)] and subharmonic generation [due to period-doubling bifurcations (PDB's)] are not as ubiquitous features of driven classical nonlinear systems with dissipation as is superharmonic generation. These bifurcations usually require the fine-tuning of parameters, but have many important applications.[1,2] The same bifurcations may exist and require fine-tuning in some driven quantum mechanical systems with dissipation. In a mean-field description, Bose-Einstein condensates,[3] Josephson junctions,[4,5] atomic beams in optical cavities,[6] and $n$-doped quantum wells[7] (QW's) have nonlinear equations of motion. This necessitates a theoretical search for the appropriate parameter ranges in which these systems could have an essentially nonlinear response. We will focus on strongly driven FIR intersubband transitions in $n$-$\delta$-doped GaAs/AlGaAs QW's which have been shown to exhibit superharmonic generation and nonlinear phenomena in their absorption line shapes. In this study we show that intersubband transitions can produce strong subharmonic and incommensurate-frequency responses to the FIR drive.

The source of the nonlinearities is many-body interactions that become much more prominent in wide QW's ($\approx$300 Å) where the intersubband spacing is $\approx$10 meV—roughly the energy of electron-electron Coulomb interactions. The absorption-peak frequency is blueshifted by dynamic shielding by the electron gas against the incoming radiation. This depolarization shift also generates second harmonics of the drive frequency when it is at half the dressed frequency.[8] The shift and superharmonic generation have been accurately simulated and measured.[8–11] In addition there is a dynamic Stark shift of the absorption peak proportional to the intensity of the incoming radiation. Experiments[8,12,13] showed the intersubband absorption peak broadening, distorting, and redshifting towards the bare intersubband frequency as it saturates with increasing far-infrared (FIR) intensity. These results are in good agreement with a two-subband density matrix model of Zalużny.[14,15]

The generic bifurcation from a fixed point (corresponding to a periodic orbit) in a classical system is a HB,[16] and it leads to a period-1 torus orbit (which corresponds to a quasiperiodic orbit defined by the incommensurate and fundamental frequencies); the magnitude of the incommensurate response can also be of the same order as the magnitude of the harmonic. This motivates the search for a strong response (a HB from a fixed point) in our effectively nonlinear quantum mechanical system that is a second frequency response of the collective electron excitations incommensurate with the frequency of the laser drive. In this study we report the existence of HB's in an $n$-$\delta$-doped QW driven by intense FIR radiation. We also extend the work of Galdrikian and Birnir[9] and of Batista *et al.*[17] on PDB's in a two-subband QW. The present model allows more subbands and in principle can also include exchange-interaction terms and mass dispersion. On the other hand, analytical calculations such as the averaging technique used in Ref. 17 are considerably more difficult to perform when more than two subbands are included. Thus, we here focus on numerical results for the nonlinear dynamics.

Many-body effects on intersubband transitions and optical properties of QW's have been studied in recent years with the semiconductor Bloch equation (SBE) using Hartree-Fock and rotating-wave approximation (RWA) for the response of two-(sub)band QW's.[7,18–21] Numerical integration of the multisubband SBE was performed by Tsang *et al.*,[22] although they neglected depolarization-shift terms, which is a serious handicap for their predictions for wide QW's.

We study the SBE associated with intersubband transitions from a nonlinear dynamical-systems perspective and *without* the RWA. We find, in qualitative agreement with previous work,[9] that for two-subband double QW's driven near resonance period-2 orbits (created through direct PDB's) (Ref. 17) and optical bistability (hysteresis) (Ref. 23) associated with saddle-node bifurcations (SNB's) may occur as the FIR field strength is varied. For the three-subband triple QW designed for this project we also find HB's besides these two types of bifurcations. When this QW is driven at resonance with $E_{20}$ (the intersubband energy $E_2 - E_0$), for some values of the field strength we observe a strong response signal at a frequency lower than the frequency of the drive. This signal corresponds to a dressing of $E_{10}-E_{21}$ and is created through HB's. For other values of the field strength strong subharmonic-response signals are observed. When the triple QW is driven in resonance with $E_{10}$ the only bifurcations observed are of the Hopf type. All of these responses are produced at moderate values of the field strength. The period-2 signal observed in the double QW in Ref. 9 was much weaker than the fundamental and occurred at relatively large field strengths. Our approach can be applied to any multisubband systems, but in practice when $\omega \geqslant E_{30}$ one may run into problems such as coupling the system to the continuum or the excitation of LO phonons (if $\omega > 36$ meV).[24]

The optical properties of the confined electrons in the QW can be studied with the many-body Hamiltonian written in terms of spinless fermion field operators. We assume that the conduction-subband effective masses are identical, which is fairly accurate for GaAs/AlGaAs QW's. The interaction with the FIR field is introduced through the electric-dipole approximation. It is also assumed that the electric field generated from the radiation off the collective oscillations inside the QW is negligible compared with the applied FIR field $\mathcal{E}$. The field operator expressed as a linear combination of annihilation operators $a_{k,n}$ is $\hat{\psi}(x,t) \equiv A^{-1/2}\Sigma_{k,n} e^{ik\cdot\rho}\xi_n(z)a_{k,n}(t)$, where $\xi_n(z)$ is the self-consistent $n$th Hartree eigenstate, $k$ is the in-plane wave vector and $A$ is the QW area.

After carefully eliminating the long-wavelength divergences in the total Hamiltonian (electrons+donors),[23,25] we obtain the Heisenberg equation within the time-dependent Hartree approximation. We neglect exchange terms since their inclusion does not qualitatively modify our results and the analysis becomes simpler. Furthermore, it has been shown[26,27] that exchange-correlation corrections on the FIR absorption lines in a double QW when two subbands are well populated are significantly reduced.

In order to be more realistic we need to introduce dissipation in our equations of motion. Since we cannot do that directly within the Heisenberg equations of motion, we use the density matrix equations, here in the time-dependent Hartree approximation. They provide the collective optical response of the electrons to the FIR field.

The equation of motion for the density matrix is

$$\begin{aligned}-i\hbar\dot{\sigma}_{n,n'} &= (E_n - E_{n'})\sigma_{n,n'} + i\Gamma_{nn'}(\sigma_{n,n'} - \sigma^0_{nn'}) \\ &\quad + \sum_{n_2n_3n_4} V^0_{n'n_2n_3n_4}\sigma_{n,n_4}(\sigma_{n_2n_3} - \sigma^0_{n_2n_3}) \\ &\quad - \sum_{n_1n_2n_3} V^0_{n_1n_2n_3n}\sigma_{n_1,n'}(\sigma_{n_2n_3} - \sigma^0_{n_2n_3}) \\ &\quad - \sum_m \mathcal{E}\cos(\omega t)(\mu_{mn}\sigma_{mn'} - \mu_{n'm}\sigma_{nm}), \quad (1)\end{aligned}$$

where $\sigma_{n,n'} = (AN_s)^{-1}\Sigma_k\langle a^\dagger_{k,n}a_{k,n'}\rangle$, $\langle\cdot\rangle$ denotes the quantum statistical average, $\sigma^0_{nn'}$ is the equilibrium density matrix ($\sigma^0_{00} = 0.68$, $\sigma^0_{11} = 0.32$), and the depolarization-shift coefficient is

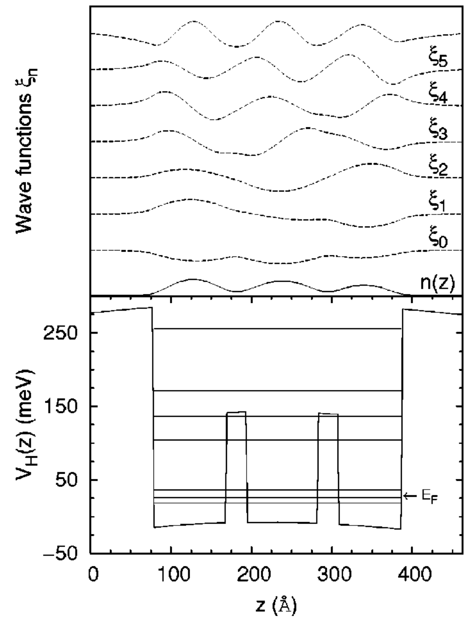


FIG. 1. The stationary self-consistent potential for $N_s = 3.0 \times 10^{11}$ cm$^{-2}$ with the eigenenergies indicated by horizontal bars; the density and the first seven eigenstates are shown on top. The double barrier creates, through tunneling, three closely spaced subbands well isolated from upper subbands. The slight asymmetry enhances the nonlinear effects, but too much asymmetry reduces the tunneling and with it the decoupling with upper subbands.

$$\begin{aligned}V^0_{n_1n_2n_3n_4} &= \frac{2\pi e^2 N_s}{\epsilon_0}\int\int \xi_{n_1}(z_1)\xi_{n_2}(z_2) \\ &\quad \times |z_1 - z_2|\xi_{n_3}(z_2)\xi_{n_4}(z_1)dz_1dz_2,\end{aligned}$$

in which $\epsilon_0 \approx 13$ is the static dielectric constant in GaAs. We introduced above, within the relaxation-time approximation, the phenomenological dissipation rates $\Gamma_{nn'} = \hbar\delta_{nn'}/T_1 + \hbar(1-\delta_{nn'})/T_2$, where $T_1$ is the energy scattering time (or depopulation time) and $T_2$ is the momentum scattering time (or depolarization time).

The GaAs/AlGaAs QW structure studied is 310 Å wide and 300 meV deep with two barrier steps of 26 Å in width and 150 meV in height. The leftmost barrier is located at 92 Å from the left edge of the QW and the distance between the two barriers is 88 Å. Figure 1 shows the effective well shape with a sheet density $N_s = 3.0\times10^{11}$ cm$^{-2}$ (provided by identical Si-$\delta$-doped donor layers set back hundreds of Å's from both sides of the QW). Equations (1) with three subbands are integrated using the fourth-order Runge-Kutta method with 2048 steps per cycle of drive. After an equilibration time of 2000 cycles of the FIR field, the data (plotted in Figs. 2–5) were taken over 128 cycles. These results are obtained at the temperature $T=0$, but we verified that they are approximately the same for $T$ up to 50 K; the nonlinearity is substantially reduced for $T>100$ K. In the first example (Figs. 2 and 3) the applied FIR field has frequency $\omega = E_{20}$, which is $\approx 5$ THz (or 20 meV) and is well in the range of the FEL (however, $E_{20}$ can be lowered by decreasing the tunneling if necessary). We found that when $N_s \approx 3.0\times10^{11}$ cm$^{-2}$ the bi-

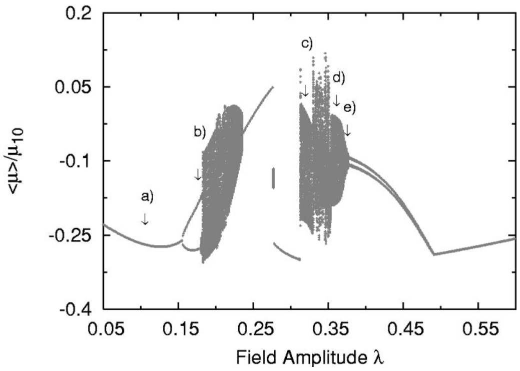


FIG. 2. The Poincaré-map bifurcation diagram of the scaled dipole moment. As the FIR field amplitude increases a range of dynamical responses occurs: period-1, period-2, period-1 torus, period-1, period-1 torus, chaotic, period-2 torus, period-2, and period-1 orbits. $\lambda = 0.1$ corresponds to $\approx 2.4$ kV/cm.

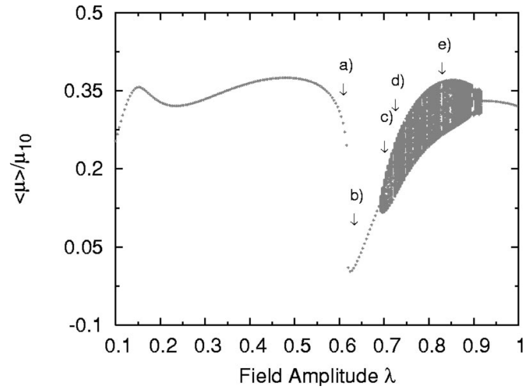


FIG. 4. As the FIR field amplitude increases an interval of optical bistability response occurs near $\lambda = 0.62$ (not shown), and a direct Hopf bifurcation occurs at $\lambda = 0.69$ with period-1 torus orbits following. $\lambda = 0.1$ corresponds to $\approx 1.3$ kV/cm and $N_s = 1.5 \times 10^{11}$ cm$^{-2}$.

furcations occur with the greatest strength and at the same time require a small field amplitude, while for $N_s < 0.5 \times 10^{11}$ cm$^{-2}$ and for $N_s > 6.0 \times 10^{11}$ cm$^{-2}$ the bifurcations become too small for practical observations. The relaxation times used were $T_1 = T_2 = 65.8$ ps ($\Gamma_1 = \Gamma_2 = 0.01$ meV). We also verified that the HB's still occur for a $T_2$ as low as 6.58 ps while $T_1$ was kept at 65.8 ps. For the FIR frequency at $\omega = E_{10}$ we used $T_1 = T_2 = 6.6$ ps ($\Gamma_1 = \Gamma_2 = 0.1$ meV). Our first value of $T_1$ is roughly the same as the one measured at low FIR intensities in a two-subband QW.[10,28] Our second $T_1$ can be inferred from Ref. 10 for a field intensity of about $10^5$ W/cm$^2$ ($\lambda \approx 0.9$). Our first $T_2$ is

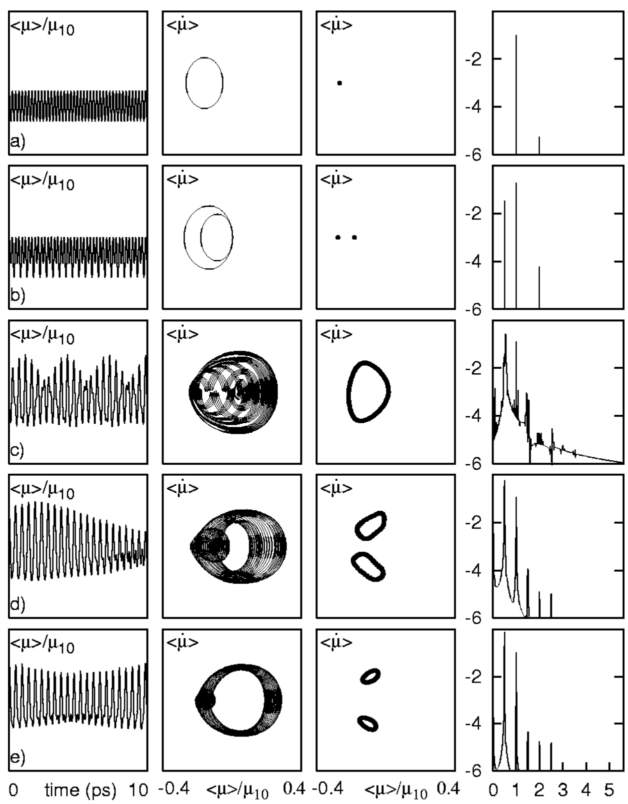


FIG. 3. Some characteristic dynamical responses. In the columns, from left to right, are shown the scaled dipole-moment time flows ($\langle \mu \rangle / \mu_{10}, \langle \dot{\mu} \rangle$), time flows ($\langle \mu \rangle / \mu_{10}, \langle \dot{\mu} \rangle$), Poincaré maps, and power spectra (in logarithmic scale) of the scaled dipole-moment time flows with frequency given in units of $\omega = E_{20}$. The corresponding values of $\lambda$ are indicated in Fig. 2.

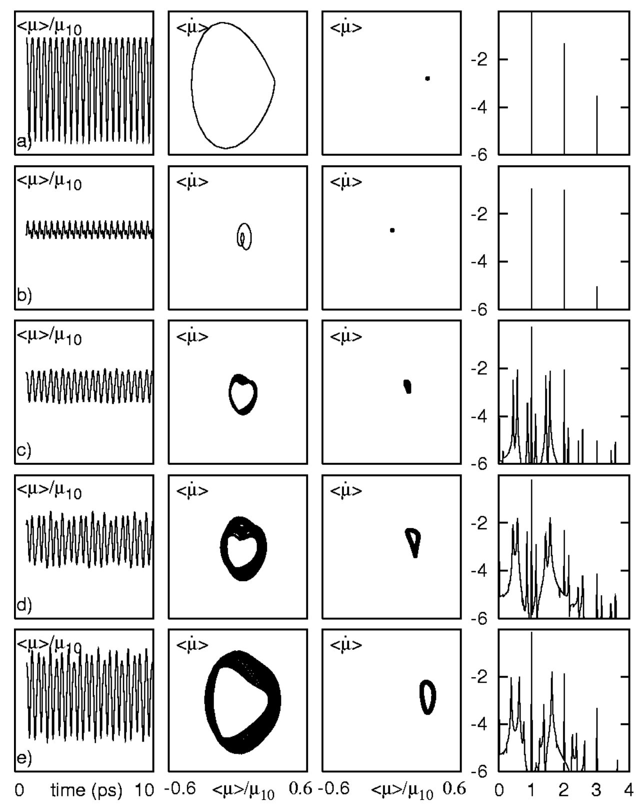


FIG. 5. Some characteristic dynamical responses. In the columns, from left to right, are shown the scaled dipole-moment time flows ($\langle \mu \rangle / \mu_{10}, \langle \dot{\mu} \rangle$), time flows ($\langle \mu \rangle / \mu_{10}, \langle \dot{\mu} \rangle$), Poincaré maps, and power spectra (in logarithmic scale) of the scaled dipole-moment time flows with frequency given in units of $\omega = E_{10}$. The corresponding values of $\lambda$ are indicated in Fig. 4.

about one order of magnitude higher than the linewidths obtained more recently in Refs. 29 and 30. Their linewidths are larger than those found in Refs. 10 and 28 and they point out that the most important contributions to them come from interface roughness of the QW walls and point impurities. One can expect then that as QW growth techniques improve these sources of scattering will be decreased and our values of $T_2$ will be approached. So far no experiments were made to determine $T_2$ for high field intensities. Also to our knowledge no experiments have been made to determine relaxation times in three- or more-subband QW's.

Below are some examples of the rich variety of dynamical behaviors our system exhibits. The bifurcation diagram in Fig. 2 describes the collective electron oscillations. It shows the Poincaré map (strobe pictures taken at the drive frequency) of the dipole-moment time flow $\langle \mu(t) \rangle = \mathrm{tr}\{\mu\sigma(t)\}$ plotted as a function of the unitless field amplitude $\lambda = e\mathcal{E}z_{10}/E_{20}$. A fixed point in this map corresponds to an orbit with the period of the drive (period 1), two points to an orbit with twice the period of the drive (period 2), a range of points filling space densely correspond to quasiperiodic or to chaotic orbits (further investigation is required to distinguish them). The results are plotted for adiabatically increasing $\lambda$. For our system $\lambda = 0.1$ corresponds to an electric field of $\approx 2.4$ kV/cm. In the $\lambda$ interval (0,0.156) period-1 orbits occur [see Fig. 3, row (c)], and at $\lambda = 0.156$ a direct PDB occurs; in (0.156,0.180) we obtain period-2 responses [see Fig. 3, row (b)], and then at $\lambda = 0.180$ a subcritical HB occurs and period-1 torus orbits appear; in (0.180,0.236) we have period-1 tori, and then they disappear and we obtain period-1 orbits again in (0.236,0.312). At $\lambda = 0.276$ a SNB occurs which causes a big jump in the response (a bistability is associated with this, seen from decreasing $\lambda$, but it is not shown here). Period-1 torus orbits occur in (0.313,0.330) [see Fig. 3, row (c)]; then, some region of apparently chaotic behavior (probably transient response due to the proximity of two attractors) in (0.330,0.353), and then in (0.354,0.378) period-2 torus orbits occur [see Fig. 3, rows (d) and (e)]. The tori decrease continuously in amplitude as $\lambda$ increases until they disappear at about $\lambda = 0.378$, which constitutes a reverse direct HB. In (0.378,0.492) we obtain period-2 orbits; they slowly decrease and disappear into a reverse direct PDB. After that we only obtain period-1 orbits.

The power spectra of the confined-electrons dipole-moment time series are shown in the last column of Fig. 3. The large and broad peak near $\omega/2$ is the main feature of the period-1 torus orbit as can be seen in Fig. 3, in row (c). This peak is broad due to the presence of the dressed energy differences $\pm(E_{21} - E_{10})$, which generate sideband peaks around it (other sidebands can also be seen close to the origin and around the harmonic peak). On the other hand, the $\omega/2$ peak for the period-2 orbits is sharp, as can be seen in row (b). For the period-2 tori, as can be seen in rows (d) and (e) of Fig. 3, the peak near $\omega/2$ becomes closer to $\omega/2$ and therefore narrower as the tori decrease in amplitude. By varying the sheet density and field strength the incommensurate peak can be tuned. It can also be changed further by increasing the QW asymmetry. The asymmetry, though, should not be too large; otherwise, the tunneling is reduced and we cannot guarantee that our three-subband QW driven at resonance with $E_{20}$ is really isolated from upper subbands and the continuum. In the power spectra of Fig. 3 we also have dc responses (rectification), but they are inside the box frames.

A period-1 orbit occurs when there are transitions only between the first and third subbands. In period-2 and in torus orbits the three subbands are active. Their increased strength in our triple QW is due to the fact that they are being assisted by the presence of almost equally spaced frequencies $E_{10}$ and $E_{21}$. In the period-2 response the dressed $E_{10}$ ($\tilde{E}_{10}$) and dressed $E_{21}$ ($\tilde{E}_{21}$) both lock at $\omega/2$. When that is not possible, as in the case of more asymmetric QW's, the only essentially nonlinear response we obtain are the period-1 torus orbits.

Finally, we would like to point out that some essentially nonlinear dynamical responses are still possible for intersubband plasmons with considerably shorter depopulation and decoherence times. For example, FIR-driven intersubband transitions in the same triple QW with $N_s = 1.5 \times 10^{11}$ cm$^{-2}$, $T_1 = T_2 = 6.6$ ps, and $\omega = \omega_{10}$ had Hopf bifurcations leading to period-1 torus orbits. Although the dynamical response is much weaker than the previous case, a direct Hopf bifurcation is still clearly seen in Fig. 4, near $\lambda = 0.7$. As expected, there is no subharmonic generation due to the nonexistence of an intersubband transition near $\omega/2$. The amplitude of the incommensurate response seen in Fig. 5, unlike the previous case, is considerably smaller than the harmonic response. This seems to be due to the fact that the process leading into the two output frequencies needs two input photons ($\tilde{E}_{10} + \tilde{E}_{21} = 2\omega$), instead of just one (at $\omega_{20}$) as before. Now the three subbands are active for period-1 orbits as well as for the torus orbits. In the period-1 response the $\tilde{E}_{10}$ and $\tilde{E}_{21}$ both lock at $\omega$, while in the torus response these dressed frequencies are different. (If $\tilde{E}_{10} = 0.8\omega$, we obtain the difference $\tilde{E}_{10} - \tilde{E}_{21} = 0.4\omega$, which is responsible for the extra peaks in the power spectra.)

As the THz region of the spectrum is opened—for science and technology—the need arises for materials and structures exhibiting nonlinearities at the FIR frequencies. The realization that QW's can undergo a Hopf bifurcation (from a periodic orbit) only observed before in (semi)classical nonlinear systems may lead to such applications as frequency downconverters for electronic detection of amplitude-modulated FIR signals and new sources.

The authors thank M. S. Sherwin and S. J. Allen for helpful discussions. The idea of nonlinear bifurcations in QW's was inspired by J. D. Crawford's elegant exposition on bifurcation theory.[31] We acknowledge Grant Nos. NSF-DMS-0072191 and DARPA-Navy and N00014-99-10935 (A.A.B. and B.B.), Proyectos UBACyT 2001-2 (P.I.T.), NSF-ECS-0072986, and the Office of Naval Research and the Yamacraw program of the State of Georgia (A.A.B. and D.S.C.).

[1] C. Holmes and P. Holmes, J. Sound Vib. **78**, 161 (1981).
[2] J. Guckenheimer and P. Holmes, *Nonlinear Oscillations, Dynamical Systems, and Bifurcations of Vector Fields* (Springer-Verlag, New York, 1983).
[3] F. Dalfovo, S. Giorgini, L.P. Pitaevskii, and S. Stringari, Rev. Mod. Phys. **71**, 463 (1999).
[4] P.W. Anderson, *Lectures on the Many-Body Problem* (Academic, New York, 1964).
[5] A.J. Leggett, Prog. Theor. Phys. Suppl. **69**, 80 (1980).
[6] P. Grangier, J.F. Roch, J. Roger, L.A. Lugiato, E.M. Pessina, G. Scandroglio, and P. Galatola, Phys. Rev. A **46**, 2735 (1992).
[7] H. Haug and S.W. Koch, *Quantum Theory of the Optical and Electronic Properties of Semiconductors* (World Scientific, Singapore, 1990).
[8] J.N. Heyman, K. Craig, B. Galdrikian, M.S. Sherwin, K. Campman, P.F. Hopkins, S. Fafard, and A.C. Gossard, Phys. Rev. Lett. **72**, 2183 (1994).
[9] B. Galdrikian and B. Birnir, Phys. Rev. Lett. **76**, 3308 (1996).
[10] J.N. Heyman, K. Unterrainer, K. Craig, B. Galdrikian, M.S. Sherwin, K. Campman, P.F. Hopkins, and A.C. Gossard, Phys. Rev. Lett. **74**, 2682 (1995).
[11] M.S. Sherwin, K. Craig, B. Galdrikian, J.N. Heyman, A. Markelz, K. Campman, S. Fafard, P.F. Hopkins, and A.C. Gossard, Physica D **83**, 229 (1995).
[12] K. Craig, B. Galdrikian, J.N. Heyman, A.G. Markelz, J.B. Williams, M.S. Sherwin, K. Campman, P.F. Hopkins, and A.C. Gossard, Phys. Rev. Lett. **76**, 2382 (1996).
[13] M.S. Sherwin, Curr. Opin. Solid State Mater. Sci. **3**, 191 (1998).
[14] M. Załużny, Phys. Rev. B **47**, 3995 (1993).
[15] M. Załużny, J. Appl. Phys. **74**, 4716 (1993).
[16] The Hopf bifurcation is well known to be related to the Ruelle-Takens quasiperiodic route to chaos in classical systems (Ref. 31).
[17] A.A. Batista, B. Birnir, and M.S. Sherwin, Phys. Rev. B **61**, 15 108 (2000).
[18] S.L. Chuang, M.S.C. Luo, S. Schmitt-Rink, and A. Pinczuk, Phys. Rev. B **46**, 1897 (1992).
[19] M.S.-C. Luo, S.L. Chuang, S. Schmitt-Rink, and A. Pinczuk, Phys. Rev. B **48**, 11 086 (1993).
[20] D.E. Nikonov, A. Imamoglu, L.V. Butov, and H. Schmidt, Phys. Rev. Lett. **79**, 4633 (1997).
[21] D.E. Nikonov, A. Imamoglu, and M.O. Scully, Phys. Rev. B **59**, 12 212 (1999).
[22] L. Tsang, C. Chansungsan, and S.L. Chuang, Phys. Rev. B **45**, 11 918 (1992).
[23] A.A. Batista, P.I. Tamborenea, B. Birnir, M.S. Sherwin, and D.S. Citrin, Phys. Rev. B **66**, 195325 (2002).
[24] These problems can be avoided by introducing more barriers in the well which create several closely spaced subbands as in Fig. 1.
[25] A.A. Batista, P.I. Tamborenea, B. Birnir, and D.S. Citrin, IEEE J. Sel. Top. Quantum Electron. **8**, 464 (2002).
[26] R. Decca, A. Pinczuk, S. Das Sarma, B.S. Dennis, L.N. Pfeiffer, and K.W. West, Phys. Rev. Lett. **72**, 1506 (1994).
[27] P.I. Tamborenea and S. Das Sarma, Phys. Rev. B **49**, 16 821 (1994).
[28] J.B. Williams, K. Craig, M.S. Sherwin, K. Campman, and A.C. Gossard, Physica E (Amsterdam) **2**, 177 (1998).
[29] J.B. Williams, M.S. Sherwin, K.D. Maranowski, and A.C. Gossard, Phys. Rev. Lett. **87**, 037401 (2001).
[30] C.A. Ullrich and G. Vignale, Phys. Rev. Lett. **87**, 037402 (2001).
[31] J.D. Crawford, Rev. Mod. Phys. **63**, 991 (1991).